Available online at www.sciencedirect.com
SCIENCE DIRECT®
Surface Science 540 (2003) 12–22
SURFACE SCIENCE
www.elsevier.com/locate/susc

Kinetics of phosphine adsorption and phosphorus desorption from gallium and indium phosphide (0 0 1)

Y. Sun, D.C. Law, R.F. Hicks *

Department of Chemical Engineering, University of California (UCLA), 405 Hilgard Avenue, Los Angeles, CA 90095-1592, USA

Received 11 October 2002; accepted for publication 5 June 2003

Abstract

The kinetics of phosphine adsorption and phosphorus desorption from gallium and indium phosphide (0 0 1) has been determined using reflectance difference spectroscopy to monitor the phosphorus coverage in real time. Assuming a Langmuir adsorption mechanism, phosphine exhibited an initial reactive sticking coefficient at 500 °C of $8.7 \pm 1.0 \times 10^{-2}$, $3.5 \pm 1.0 \times 10^{-2}$ and $1.0 \pm 0.2 \times 10^{-3}$ on the GaP (2×4), GaP (1×1) and InP (2×4) reconstructions, respectively. The sticking coefficient increased with temperature on the gallium phosphide surfaces, exhibiting an activation energy of 0.5 ± 0.2 eV, while on indium phosphide, no temperature dependence was observed. The desorption of phosphorus from the GaP (2×1) surfaces was first-order in coverage with rate constants of 5.0×10^{15} $(s^{-1}) \exp(-2.6 \pm 0.2\ (eV)/kT)$. These results may be used to estimate the feed rate of phosphine relative to the group III precursors during the metalorganic vapor-phase epitaxy of gallium and indium phosphide.

Keywords: Gallium phosphide; Indium phosphide; Phosphine; Adsorption kinetics; Sticking

1. Introduction

Compound semiconductor devices, such as edge-emitting lasers, heterojunction bipolar transistors and multi-junction solar cells, are composed of thin films of gallium arsenide, gallium phosphide, indium arsenide, indium phosphide, and alloys thereof [1–4]. These materials are deposited by metalorganic vapor-phase epitaxy (MOVPE), using volatile precursors of the group III and V elements [5–7]. The feed rates of the precursors are carefully controlled in order to achieve lattice matching of the alloy films to their binary counterparts. This is particularly true for $In_xGa_{1-x}As_yP_{1-y}$, where it is found that the y value in the alloy follows a nonlinear dependence on the ratio of the group V precursors fed to the reactor [6,8–10]. For example, when only a small amount of arsenic is required in the film, the alloy composition is very sensitive to the phosphine addition rate.

The nonlinear dependence of the alloy composition on the concentrations of the group V precursors in the gas is due to the fact that the decomposition rates of these species are controlled by heterogeneous chemical reactions [5,6]. The principal surface reactions occurring during MOVPE are (1) the irreversible adsorption of arsine and

* Corresponding author. Tel.: +1-310-206-6865; fax: +1-310-206-4107.
E-mail address: rhicks@ucla.edu (R.F. Hicks).

0039-6028/$ - see front matter © 2003 Elsevier B.V. All rights reserved.
doi:10.1016/S0039-6028(03)00834-3

phosphine; and (2) the desorption of arsenic and phosphorus. It has been found that group V-rich surfaces prevent the incorporation of undesired impurities in the films, so to insure this condition during growth, V/III feed ratios between 10 and 500 are employed [7,8,11,12].

In this work, we have determined the kinetics of phosphine adsorption and phosphorus desorption from gallium and indium phosphide (0 0 1) at surface coverages ranging from 0.13 to 1.00 monolayers (ML) of phosphorus. These experiments were carried out on MOVPE-grown surfaces in well-controlled ultrahigh vacuum (UHV) conditions. Changes in the P coverage during isothermal adsorption and desorption were recorded using reflectance difference spectroscopy. By solving the mass balances for the adsorbed phosphorus on the different reconstructions, we were able to extract the heterogeneous reaction kinetics from these data. It was found that the sticking probability of phosphine is higher on gallium phosphide than on indium phosphide, while the rate of phosphorus desorption is lower on the former surface compared to the latter one. These data can explain why relatively high V/III feed ratios are used during the MOVPE of these materials.

2. Experimental methods

Gallium and indium phosphide films, approximately 0.5 μm thick, were deposited on nominally flat GaP and InP(0 0 1) substrates in a horizontal MOVPE reactor. The hydrogen carrier gas was passed through a SAES Pure Gas hydrogen purifier PS4-MT3-H to remove any oxygen, nitrogen or hydrocarbon contamination. The total reactor pressure was 20 Torr and the substrate temperature was 585 and 565 °C for GaP and InP growth. Trimethylgallium, trimethylindium, and tertiarybutylphosphine (TBP) were introduced to the reactor at partial pressures of 1.3×10^{-4}, 6.5×10^{-4}, and 1.3×10^{-1} Torr, respectively. After deposition, the TBP flow and the H_2 flow were maintained until the samples were cooled to 300 and 40 °C, respectively. Then the crystals were transferred directly to an UHV system for surface analysis.

Inside the UHV chamber the gallium phosphide samples were heated to 300 or 550 °C for 20 min to create either a (2×1), or a (2×4) reconstruction. For indium phosphide, the (2×1) and (2×4) structures were generated by annealing at 300 and 450 °C for 20 min. After cooling the samples to 25 °C, the long range ordering on the surfaces was characterized by low-energy electron diffraction (LEED). In addition, reflectance difference spectra of the surface reconstructions were recorded with an Instruments SA J-Y Nisel RD spectrometer [13–15]. The measured signal, $Re(\Delta R/R)$, corresponded to the difference in the real part of the optical reflectance measured along the $[\bar{1}\,1\,0]$ and $[1\,1\,0]$ crystal axis, i.e., $[(R_{[\bar{1}\,1\,0]}-R_{[1\,1\,0]})/\langle R\rangle]$. Baseline drift was subtracted from the data by taking the average of two spectra collected with the polarizer oriented +45° and −45° relative to the $[\bar{1}\,1\,0]$.

Reflectance difference signals were recorded at specific energies (see below) during the isothermal adsorption of phosphine or desorption of phosphorus. First the samples were annealed to produce the group III-rich (2×4) reconstructions. Then the temperature was adjusted to a desired value, and phosphine was introduced through a leak valve at pressures ranging from 10^{-7} to 10^{-4} Torr for times ranging from 5 to 15 min. The pressures were measured using an ion gauge filament that was corrected with a known calibration factor [16]. Conversely, isothermal desorption data were taken immediately after closing the leak valve at background pressures below 10^{-9} Torr. Periodically during these measurements, the surface structure was checked by LEED. All the experiments were conducted at phosphorus coverages between 0.13 and 1.00 ML [13,14].

3. Results

3.1. Data analysis

Previous studies have shown that the gallium phosphide (0 0 1) surface exhibits three stable reconstructions, the $\delta(2\times4)$, (1×1) and (2×1) [13,17]. As shown in Table 1, these structures are covered with 0.13, 0.67 and 1.00 ML of phosphorus. On the other hand, the indium phosphide

Table 1
Surface structures observed on GaP and InP(0 0 1) [13,15,18]

Surface phases	GaP			InP		
	$\delta(2\times4)$	(1×1)	(2×1)	$\delta(2\times4)$	$\sigma(2\times4)$	(2×1)
P coverage	0.13	0.67	1.00	0.13	0.25	1.00
Ga/In coverage	0.87	0.33	0.00	0.87	0.75	0.00

(0 0 1) surface may be terminated with $\delta(2\times4)$, $\sigma(2\times4)$, or (2×1) phases with P coverages of 0.13, 0.25, or 1.00 ML, respectively [18–20]. Under super-P-rich conditions, a mixed (2×1) and (2×2) reconstruction is formed with between 1.00 and 1.50 ML of phosphorus [19]. In this study, the (2×2) phase is not examined.

Shown in Fig. 1 are reflectance difference spectra of the (2×1), (1×1) and (2×4) reconstructions of GaP(0 0 1) recorded at 500 °C. The spectrum of the (2×1) contains a series of weak negative bands between 1.7 and 2.7 eV, and two positive peaks at 3.4 and 4.9 eV. The spectrum of the (1×1) exhibits several weak negative bands between 1.7 and 2.5 eV, and two positive peaks at 3.3 and 4.9 eV. For the (2×4), one observes an intense negative peak at 2.2 eV, a shoulder at 2.5 eV, and positive bands at 3.2, 3.8 and 4.9 eV. Shown in Fig. 2 are RD spectra of the (2×1) and (2×4) reconstructions of InP(0 0 1) recorded at 400 °C. The spectrum of the (2×1) contains a negative peak at 1.7 eV, an intense positive peak at 2.9 eV, and a broad asymmetric band centered at 4.0 eV. By contrast, the spectrum of the (2×4) exhibits a broad negative band at 1.8 eV and three positive peaks at 2.7, 3.6, and 4.5 eV.

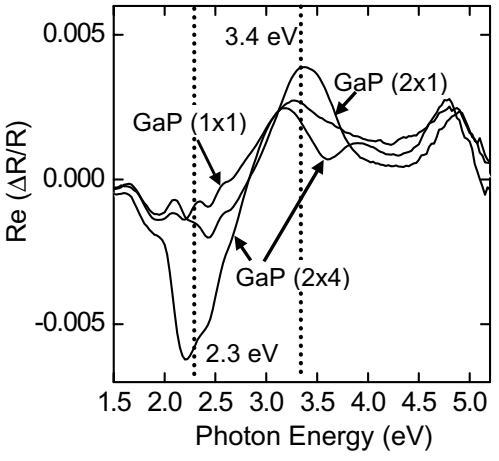

Fig. 1. Reflectance difference spectra of the GaP(0 0 1)-(2×1), (1×1) and (2×4) reconstructions at a substrate temperature of 500 °C.

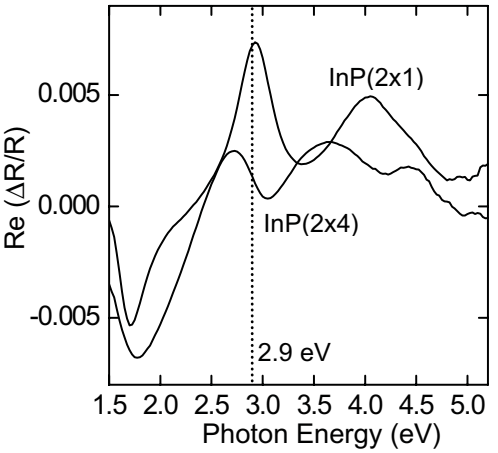

Fig. 2. Reflectance difference spectra of the InP(0 0 1)-(2×1) and (2×4) reconstructions at a substrate temperature of 400 °C.

We have found that the RD spectra of mixed-phase GaP or InP(0 0 1) surfaces are linear combinations of the spectra of the pure phases [13,14]. In other words, the fraction, x, of $(m\times n)$ present on a surface that contains $(m\times n)$ and $(r\times q)$ reconstructions may be determined from the following equation:

$$\Delta R/R_{\text{mixed}} = x\cdot\Delta R/R_{(m\times n)} + (1-x)\cdot\Delta R/R_{(r\times q)} \tag{1}$$

The validity of Eq. (1) has been established by benchmarking the optical spectra against scanning tunneling micrographs and X-ray photoemission spectra of the surfaces. To measure the fraction of $(m\times n)$ in real time, one only needs to monitor the RD signal at a specific energy where there is a maximum difference in signal between the $(m\times n)$ and $(r\times q)$ reconstructions.

Referring to Fig. 1, we have found that fractions of (2×4) and (2×1) phases present on GaP(0 0 1) are best assessed by tracking the RD signal intensity at 2.3 and 3.4 eV. Both of these positions attain low absolute intensities when the surface is terminated with the (1×1) phase. In particular, the fractional coverages of the (2×4) and (2×1) are determined from the following equations [13]:

$$\theta_{(2\times4)} = \left(\frac{I_s - I_{(1\times1)}}{I_{(2\times4)} - I_{(1\times1)}}\right)_{2.3\text{ eV}} \tag{2}$$

and

$$\theta_{(2\times1)} = \left(\frac{I_s - I_{(1\times1)}}{I_{(2\times1)} - I_{(1\times1)}}\right)_{3.4\text{ eV}} \tag{3}$$

where I is the intensity of the RD signal at 2.3 or 3.4 eV, and the subscripts s, (1×1), (2×4) and (2×1) correspond to the sample surface, the pure (1×1), the pure (2×4) and the pure (2×1) phases, respectively. Finally, the fractional coverage of the (1×1) is obtained from the conservation equation:

$$\theta_{(1\times1)} = 1.0 - \theta_{(2\times4)} - \theta_{(2\times1)} \tag{4}$$

It is estimated that the error in calculating the coverage of each phase from Eqs. (2)–(4) is no more than 15% of the value.

Referring to Fig. 2, the reflectance signal at 2.9 eV is best used to monitor the fraction of the indium phosphide (0 0 1) surface covered with the (2×1) phase [14]:

$$\theta_{(2\times1)} = \left(\frac{I_s - I_{(2\times4)}}{I_{(2\times1)} - I_{(2\times4)}}\right)_{2.9\text{ eV}} \tag{5}$$

A balance for this surface yields:

$$\theta_{(2\times4)} = 1.0 - \theta_{(2\times1)} \tag{6}$$

In Eqs. (5) and (6), no distinction is made whether the (2×4) is of the σ or δ type with P coverages of 0.25 or 0.13 ML, respectively. This is because the reflectance difference spectra for these two reconstructions are identical [14].

Based on the information presented in Table 1, the phosphorus coverage can be calculated from the fractions of each reconstruction present on the surface. For gallium phosphide we have

$$\theta_P = 0.125 \cdot \theta_{(2\times4)} + 0.67 \cdot \theta_{(1\times1)} + 1.0 \cdot \theta_{(2\times1)} \tag{7}$$

And for indium phosphide we have

$$\theta_P = 0.2 \cdot \theta_{(2\times4)} + 1.0 \cdot \theta_{(2\times1)} \tag{8}$$

In Eq. (8), the 0.2 weighting factor is obtained by averaging the phosphorus coverages of the $\sigma(2\times4)$ and $\delta(2\times4)$ phases. Less than 15% error in the coverage is introduced by this approximation [14]. Note that θ_P is a minimum on the $\delta(2\times4)$ reconstruction. Further heating to desorb material from this surface will result in congruent evaporation.

Exposing gallium phosphide (0 0 1) to phosphine at high temperatures (>400 °C), leads to the following reactions:

$$(2\times4) \underset{+1}{\overset{-1}{\leftrightarrows}} (1\times1) \underset{+2}{\overset{-2}{\leftrightarrows}} (2\times1) \tag{9}$$

Phosphine adsorption sequentially converts the (2×4) to the (1×1) to the (2×1), whereas phosphorus desorption reverses this sequence. Batch material balances on these three reconstructions are given by

$$\frac{d\theta_{(2\times4)}}{dt} = -R_{+1} + R_{-1} \tag{10}$$

$$\frac{d\theta_{(1\times1)}}{dt} = R_{+1} - R_{-1} - R_{+2} + R_{-2} \tag{11}$$

$$\frac{d\theta_{(2\times1)}}{dt} = R_{+2} - R_{-2} \tag{12}$$

where R_{+1} and R_{+2} are the phosphine adsorption rates (s^{-1}), and R_{-1} and R_{-2} are the phosphorus desorption rates (s^{-1}).

Similarly, when indium phosphide (0 0 1) is dosed with phosphine at elevated temperatures, the following reaction occurs:

$$(2\times4) \underset{+3}{\overset{-3}{\leftrightarrows}} (2\times1) \tag{13}$$

A mass balance on the (2×1) phase during this process is given by

$$\frac{d\theta_{(2\times1)}}{dt} = R_{+3} - R_{-3} \tag{14}$$

where R_{+3} is the phosphine adsorption rate (s^{-1}), and R_{-3} is the phosphorus desorption rate (s^{-1}).

In the following paragraphs, we describe specific adsorption and desorption scenarios that were examined in this work. Due to the experimental

conditions used, some of the reaction rates could be neglected, leading to simpler mass balances with analytical solutions. It is assumed that all the reaction rates obey a first-order dependence on the fraction of the phase that is present on the surface. This approximation is justified in Section 4.

Case 1: Adsorption without phosphorus desorption

Below 500 °C, the amount of phosphorus on the GaP surface remains constant even without supplying any phosphine to the vacuum chamber. Thus, the phosphorus desorption rates, R_{-1} and R_{-2} may be omitted from Eqs. (10)–(12). A Langmuir adsorption mechanism is assumed, where the first-order rate constant k_{+i} is associated with the initial sticking coefficient of PH_3 on GaP(0 0 1) (See below in Eq. (23)). Integrating these mass balances with respect to time yields the following expressions for the fractional coverages of the three surface phases, when the initial condition is $\theta_{(2\times4)} = 1.0$:

$$\theta_{(2\times4)} = e^{-k_{+1}t} \tag{15}$$

$$\theta_{(1\times1)} = \left(\frac{k_{+1}}{k_{+1}-k_{+2}}\right)(e^{-k_{+2}t} - e^{-k_{+1}t}) \tag{16}$$

$$\theta_{(2\times1)} = \left(1 + \frac{k_{+2}}{k_{+1}-k_{+2}}e^{-k_{+1}t} - \frac{k_{+1}}{k_{+1}-k_{+2}}e^{-k_{+2}t}\right) \tag{17}$$

where k_{+1} and k_{+2} are the "first-order" adsorption rate constants (s^{-1}). Similar expressions may be derived for indium phosphide, when phosphine dosing is carried out below 400 °C. In this case, Eq. (14) may be integrated with an initial condition of $\theta_{(2\times4)} = 1.0$:

$$\theta_{(2\times1)} = 1 - e^{-k_{+3}t} \tag{18}$$

Here k_{+3} is the rate constant for phosphine adsorption on InP(0 0 1)-(2×4) (s^{-1}).

Case 2: Desorption without adsorption on GaP(0 0 1)

If phosphorus desorption occurs from a P-rich surface in the absence of phosphine, Eq. (12) may be integrated to give:

$$\theta_{(2\times1)} = \theta^{o}_{(2\times1)}e^{-k_{-2}t} \tag{19}$$

where $\theta^{o}_{(2\times1)}$ is the initial coverage of the (2×1) structure on the GaP or InP surface. Over a narrow range of temperatures, from 500 to 550 °C, we have found that the GaP (2×1) decomposes into the (1×1), but that no further phosphorus desorption occurs for over 8 h, so that $\theta_{(2\times4)}$ is ~0.0. In this case, Eq. (19) may be substituted into Eq. (4) to generate:

$$\theta_{(1\times1)} = 1 - \theta^{o}_{(2\times1)}e^{-k_{-2}t} \tag{20}$$

Case 3: Desorption with adsorption on GaP(0 0 1)

At temperatures above 540 °C, phosphorus desorption from GaP(0 0 1) was carried out with 1.0×10^{-8} Torr phosphine in the background gas. This was done to prevent evaporation and degradation of the crystal surface. Under these experimental conditions, only the (1×1) and (2×4) phases were present on the surface, so that R_{+2} and R_{-2} may be neglected in Eqs. (10) and (11). When the initial condition is $\theta_{(1\times1)} = 1.0$, integrating these equations with respect to time gives:

$$\theta_{(2\times4)} = \left(\frac{k_{-1}}{k_{+1}+k_{-1}}\right)[1 - e^{-(k_{+1}+k_{-1})\cdot t}] \tag{21}$$

$$\theta_{(1\times1)} = 1 - \left(\frac{k_{-1}}{k_{+1}+k_{-1}}\right)[1 - e^{-(k_{+1}+k_{-1})\cdot t}] \tag{22}$$

The integral mass balances presented above may now be used to analyze the changes in surface coverages recorded by the RDS technique during the isothermal adsorption and desorption experiments.

3.2. Phosphine adsorption on GaP(0 0 1)

Presented in Fig. 3 are the dependencies of the (2×4), (1×1), and (2×1) surface fractions on time during exposure of the GaP(0 0 1)-(2×4) surface to 5.0×10^{-5} Torr phosphine at 435 °C. The phosphorus coverage calculated from Eq. (7) is displayed as well. Upon introducing the PH_3 at 95 s, the (2×4) coverage rapidly declines, exhibiting a first-order exponential decay function. This is followed by the growth of the (1×1) and the (2×1) surface phases. The (1×1) coverage reaches a maximum value of 0.45 at 107 s, and thereafter

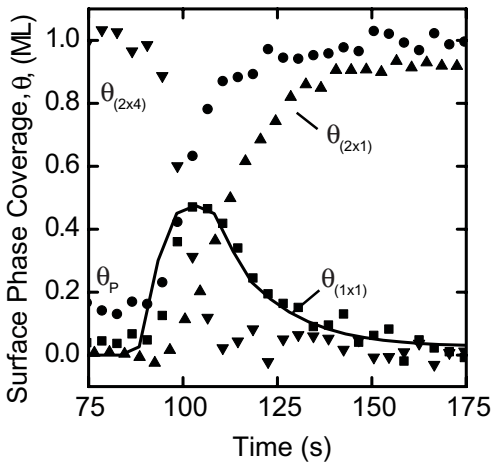

Fig. 3. The dependence of the fractional coverages of the (2×4), (1×1) and (2×1) phases and of the phosphorus coverage on time during exposure of the GaP(0 0 1) surface to 5×10^{-5} Torr PH_3 at 435 °C.

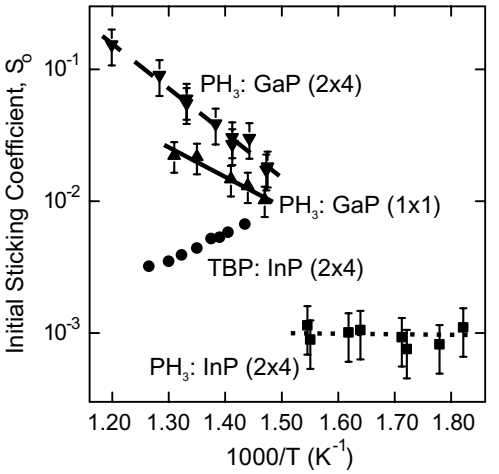

Fig. 4. The dependence of the zero-coverage sticking coefficient on inverse temperature for phosphine adsorption on the GaP (2×4), GaP (1×1) and InP (2×4) surfaces, and for TBP adsorption on the InP (2×4) surface [15].

falls at a somewhat slower rate than is observed initially for the (2×4).

The solid lines in Fig. 3 are the best fit of Eqs. (15)–(17) to the experimental data. From the fit, the rate constants, k_{+1} and k_{+2}, are found to be 0.018 and 0.008 s^{-1}. These first-order rate constants are related to the initial sticking probability of phosphine on GaP(0 0 1) by

$$k_n = \frac{\frac{1}{4}\cdot v \cdot N_{PH_3}\cdot S_0}{N} \tag{23}$$

where v is the mean molecular speed of PH_3 (cm/s), S_0 is the initial sticking coefficient of phosphine, N_{PH_3} is the number concentration of PH_3 molecules in the gas phase (cm^{-3}), N is the GaP (1×1) site concentration (6.7×10^{14} cm^{-2}), and the subscript n is either +1 or +2. The initial sticking coefficients for PH_3 on the (2×4) and (1×1) reconstructions are calculated to be 0.030 and 0.015 at 435 °C.

The above experiment was repeated at a series of temperatures between 400 and 500 °C, each time determining the zero-coverage sticking coefficients on the GaP (2×4) and (1×1) surfaces. In Fig. 4, the logarithms of S_{0+1} and S_{0+2} are plotted against the inverse temperature. It is seen that the sticking coefficients range from about 0.01–0.1, and they increase with increasing temperature. From the slopes and intercepts of the two lines, S_{0+1} equals $840.0\exp(-0.6\pm0.2$ eV/kT), while S_{0+2} equals $18.0\exp(-0.4\pm0.2$ eV/kT).

3.3. Adsorption on InP(0 0 1)

Phosphine adsorption experiments were performed on the InP(0 0 1)-(2×4) surface at temperatures ranging from 270 to 370 °C. The results of this work, in addition to an earlier study on TBP adsorption on indium phosphide, are shown in Fig. 4. The kinetic constants determined from these data are presented in Table 2 as well. It is seen that the initial sticking probability of PH_3 on InP(0 0 1)-(2×4) is approximately 0.001 between 270 and 370 °C, which is lower than that recorded for PH_3 adsorption on GaP(0 0 1)-(2×4). A comparison of the results obtained for TBP to that for PH_3 reveals several important differences between the two precursors. First, the reactive sticking probability is 3–10 times larger for the former molecule on indium phosphide. Secondly, the sticking probability of TBP decreases with increasing temperature, while the sticking probability of phosphine is constant or slightly increasing with temperature.

Table 2
Kinetic parameters for phosphine adsorption and phosphorus desorption from GaP and InP(0 0 1)

Reaction	Pre-exponential factor	Energy barrier (eV)	Rate constant at 550 °C
Phosphine adsorption			S_0
GaP (2×4)	7.3×10^{2}	0.6 ± 0.2	$1.2\ (\pm0.8)\times10^{-1}$
GaP (1×1)	1.6×10^{1}	0.4 ± 0.2	$4.2\ (\pm3.0)\times10^{-2}$
InP (2×4)	5.5×10^{-3}	0.1 ± 0.2	$1.3\ (\pm0.9)\times10^{-3}$
InP (2×4)[a,b]	1.0×10^{-5}	-0.4 ± 0.1	$2.8\ (\pm1.8)\times10^{-3}$
Phosphorus desorption	(s^{-1})		k_{-n} (s^{-1})
GaP (2×1)	5.0×10^{15}	2.6 ± 0.2	$7.2\ (\pm4.5)\times10^{-1}$
GaP (1×1)	–	–	$1.4\ (\pm0.7)\times10^{-2}$
InP (2×1)[b]	5.0×10^{14}	2.4 ± 0.2	$1.2\ (\pm1.0)\times10^{0}$

[a] TBP adsorption instead of phosphine adsorption.
[b] From Ref. [15].

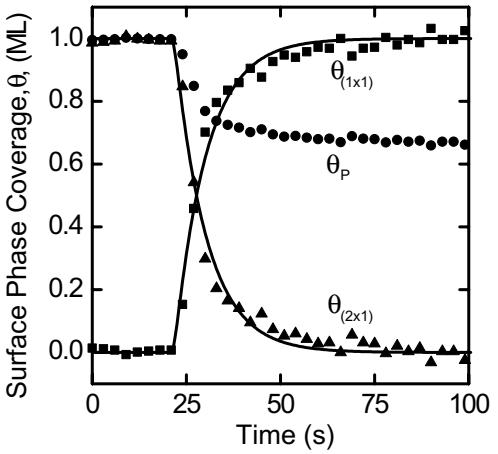

Fig. 5. The dependence of the fractional coverages of the (2×1) and (1×1) phases and of the phosphorus coverage on time during phosphorus desorption from the GaP(0 0 1) surface at 510 °C.

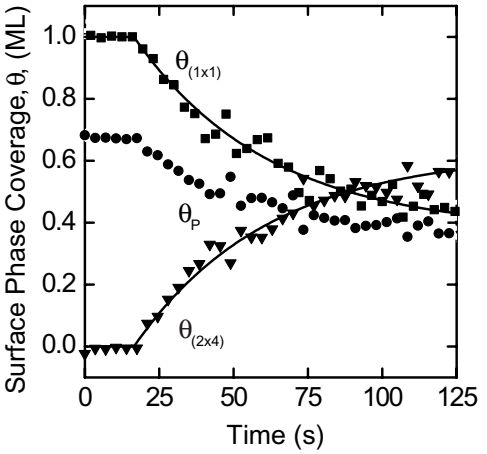

Fig. 6. The dependence of the fractional coverages of the (1×1) and (2×4) phases and of the phosphorus coverage on time during phosphorus desorption from the GaP(0 0 1) surface at 550 °C.

3.4. Phosphorus desorption from GaP(0 0 1)

Shown in Fig. 5 are desorption curves for phosphorus from the GaP(0 0 1)-(2×1) reconstruction at 510 °C. Desorption began at 25 s, which is the point when the phosphine pressure in the chamber was reduced to zero. An exponential decrease in the (2×1) coverage is observed simultaneously with an exponential increase in the (1×1) coverage. At this temperature, the (1×1) phase is stable in vacuum, so no significant amount of the (2×4) structure was detected by RDS. This situation corresponds to Case 2 above. Accordingly, the solid lines in Fig. 5 are the best fit of Eqs. (19) and (20) to the experimental data, and they yield a first-order rate constant for phosphorus desorption, k_{-2}, of 0.052 s^{-1}.

Isothermal desorption experiments from GaP(0 0 1)-(2×1) were carried out between 485 and 535 °C. The rate constants for phosphorus desorption have been obtained as described above, and the results are presented in Fig. 7. From the slope and intercept of the line, the pre-exponential factor and activation energy for phosphorus desorption from the (2×1) reconstruction are 2.6 ± 0.2 eV and 5.0×10^{15} s^{-1}, respectively.

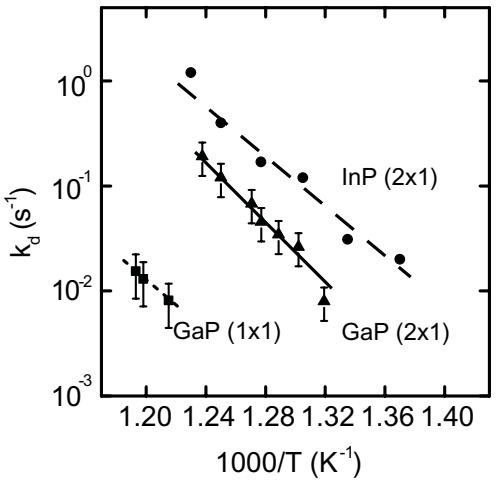

Fig. 7. The effect of temperature on the rate constants for phosphorus desorption from the GaP (2×1), GaP (1×1) and InP (2×1) reconstructions.

Upon heating the gallium phosphide crystals above 540 °C, phosphorus desorption occurs from the (1×1) converting it into the $\delta(2\times4)$ structure. Shown in Fig. 6 are the dependencies of the fractional coverages of these two surface phases on time at 550 °C. During this experiment, 1.0×10^{-8} Torr of PH_3 was supplied to the chamber to prevent GaP evaporation. This corresponds to Case 3 above. The best fits of Eqs. (21) and (22) to the data are illustrated by the solid lines in the figure. From these curves, the phosphorus desorption rate constant, k_{-1}, is found to be 0.014 s^{-1}. These measurements were repeated at three temperatures between 550 and 565 °C, and the results are plotted in Fig. 7. Due to the large experimental uncertainty, we have not calculated a pre-exponential factor and energy barrier for phosphorus desorption from the (1×1) reconstruction.

4. Discussion

The initial reactive sticking coefficients for phosphine adsorption on the GaP(0 0 1)-(2×4) and (1×1) and InP(0 0 1)-(2×4) surfaces at 550 °C are listed in Table 2. At this temperature, phosphine decomposes approximately 100 times faster on the GaP (2×4) than on the InP (2×4). The relative rate difference is larger above 550 °C due to the increasing sticking probability of PH_3 on GaP with temperature. The low S_0 for phosphine adsorption on InP, ~0.001, explains why one needs such a large excess of this source over the group III precursor during MOVPE [5,21–23]. In this regard, TBP is a more efficient group V source. Its initial reactive sticking probability is about double that of phosphine at 550 °C.

The temperature-dependent adsorption kinetics can be understood in terms of the mechanism we have proposed for the decomposition of the group V precursors on compound semiconductor surfaces [15,24–26]. A reaction scheme for phosphine adsorption on GaP(0 0 1) is expressed as follows:

$$*_{Ga} + PH_{3\,(g)} \leftrightarrows *_{Ga}PH_3 \tag{24}$$

$$*_P + *_{Ga}PH_3 \rightarrow *_PH + *_{Ga}PH_2 \tag{25}$$

$$*_{Ga}PH_2 \rightarrow *_P + \text{products} \tag{26}$$

$$*_P \rightarrow *_{Ga} + \tfrac{1}{2}P_{2\,(g)} \tag{27}$$

In the first step, the phosphine molecule forms a dative bond with the empty dangling orbital on a gallium atom exposed on the semiconductor surface. This reaction is reversible. Then, the adsorbed PH_3 molecule irreversibly decomposes by sequential dissociation and transfer of its H atoms to neighboring phosphorus sites. The first dissociation step is expected to be rate controlling [25]. At temperatures above about 350 °C, the H atoms recombine and desorb as H_2, leaving dimerized P atoms on the surface. These species can desorb as P_2 at temperatures above 500 °C, and return the surface to its initial Ga-rich state.

A qualitative potential energy diagram for the reactive adsorption of phosphine on GaP(0 0 1) is shown in Fig. 8. Dative bond formation is exothermic downhill with little or no activation barrier. It results in the release of the dative bond energy, $-\Delta H$. On the other hand, the dissociation step exhibits a significant energy barrier, E_{ra}. This pathway leads to the following temperature dependence of the reactive sticking coefficient: $S_0 = A\cdot\exp(-(E_{ra}+\Delta H)/kT)$ [15,25]. When E_{ra} is greater than $-\Delta H$, S_0 increases with temperature,

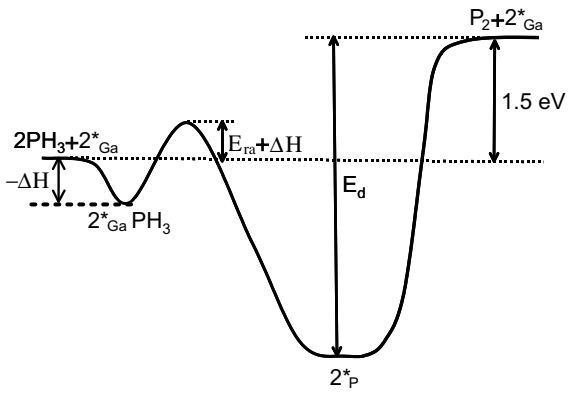

Fig. 8. Potential energy diagram for phosphine adsorption and phosphorus desorption from GaP(0 0 1).

whereas when E_{ra} is less than $-\Delta H$, S_0 decreases with temperature. For the overall decomposition of phosphine into gas-phase phosphorus dimers:

$$2PH_{3\,(g)} \rightarrow P_{2\,(g)} + 3H_{2\,(g)} \quad (28)$$

the heat of reaction is calculated to be 1.5 eV [27,28].

For phosphine adsorption on the GaP(0 0 1) surfaces, we have observed that the sticking probability increases with temperature, indicating that $E_{ra} > -\Delta H$. Within the experimental error of our measurements, the difference, $E_{ra} + \Delta H$, is the same on both (2×4) and (1×1) reconstructions, ~0.5 eV (see Table 2). These results may be contrasted with phosphine adsorption on InP(0 0 1)-(2×4), where $E_{ra} + \Delta H$ equals 0.1 eV. An examination of the adsorption kinetics for TBP reveals that this molecule exhibits a trend opposite to that observed for phosphine. The sticking rate of TBP on InP(0 0 1)-(2×4) increases with declining temperature. This means that $E_{ra} < -\Delta H$ for the organometallic molecule, which is consistent with the lower dissociation energy of the phosphorus-*t*-butyl bond compared to the P–H bond [5].

Turning our attention to the phosphorus desorption kinetics presented in Table 2, it is seen that the rate constant at 550 °C is about 70 times greater on the (2×1) compared to the (1×1). The origin of this rate difference is not clear at this time, and is probably related to the way in which the phosphorus dimers are bonded to each of these reconstructions. Whereas the structure of the (2×1) has been identified [17], the arrangement of the surface atoms on the (1×1) still needs to be determined.

A comparison of the phosphorus desorption rate constants, k_{-1} and k_{-3}, reveals that phosphorus desorbs from indium phosphide 1.7 times faster than from gallium phosphide at 550 °C. Note that the pre-exponential factor for desorption from InP is one order of magnitude lower than that for GaP, whereas the energy barriers differ by only 0.2 eV. Nevertheless, since the energy barrier is in the exponential term, it has a much larger influence on the rate. It may be concluded that enthalpic effects dominate over entropic effects, owing to the difference in the Ga–P and In–P bond energies [29].

During the MOVPE growth of compound semiconductors, it is important to maintain the surface in a group-V-rich state. Impurities such as hydrocarbons, oxygen and water rapidly decompose on group III elements that are exposed on the crystal surface, and ultimately incorporate into the

Table 3
An estimate of the V/III ratio required to keep the surface covered with 0.95 ML phosphorus during GaP or InP MOVPE[a]

Temperature (°C)	V/III ratio[b]		
	GaP with PH_3	InP with PH_3	InP with TBP
530	0.5	33	17
560	1	113	72
590	4	360	277
620	10	1060	975

[a] Calculation ignores mass-transfer phenomena in MOVPE reactor.
[b] TMGa or TMIn partial pressure of 5×10^{-4} Torr.

film [5,30]. By contrast, a group-V terminated surface is not reactive towards these species [12,30]. To maintain a group-V-rich surface during growth, it is necessary to feed to the reactor a large excess of the phosphorus source over the gallium or indium precursors. Based on the reaction kinetics reported herein, it is possible to estimate the group V partial pressure required to keep a GaP or InP (0 0 1) surface 95% covered with the (2×1) reconstruction. One simply solves Eqs. (12) and (14) under steady-state conditions with $\theta_{(2\times1)}$ set to 0.95. The group III partial pressure may be fixed at 5.0×10^{-4} Torr to yield a growth rate near 1 μm/h.

Shown in Table 3 are the V/III ratios needed to maintain a GaP or InP(0 0 1) surface 95% terminated with the (2×1) structure at different growth temperatures. This calculation does not include mass transfer and boundary layer effects that may be important in MOVPE reactors operating at 20–500 Torr [21,22]. Nevertheless, this qualitative calculation illustrates trends that are useful in understanding process operation. Namely, one sees that the V/III ratio needed for impurity-free deposition increases rapidly with temperature. This is due to the large activation barriers for phosphorus desorption from GaP and InP. Another interesting comparison is the MOVPE of indium phosphide with TBP versus PH_3. The former precursor may be introduced at a lower partial pressure than the latter one. This is consistent with several reports in the literature indicating that TBP is a more efficient source for InP epitaxy [31–33].

5. Conclusions

In summary, reflectance difference spectroscopy has been used to measure the fractional coverage of each reconstruction on the GaP and InP(0 0 1) surfaces during PH_3 adsorption and P_2 desorption. The kinetics of these reactions have been determined by solving the material balance equations for each phase, and fitting the results to the experimental data. These kinetics provide an explanation of why V/III ratios between 10 and 500 are used to grow gallium and indium phosphide thin films by MOVPE.

Acknowledgements

Funding for this research was provided by the National Science Foundation (Divisions of Chemical and Thermal Systems and Materials Research), and by TRW Inc., Emcore Corp., Epichem Inc. and the UC-SMART program.

References

[1] H.-G. Bach, W. Schlaak, G.G. Mekonnen, A. Seeger, R. Steingrüber, C. Schramm, G. Jacumeit, R. Ziegler, A. Umbach, G. Unterbörsch, W. Passenberg, W. Ebert, T. Eckardt, in: Trends in Optics and Photonics, Optical Fiber Communication Conference, vol. 37, Baltimore, MD, USA, 2000.
[2] F. Alexandre, J.L. Benchimol, J. Dangla, C. Dubon-Chevallier, V. Amarger, Electron. Lett. 26 (1990) 1753.
[3] M.T. Camargo Silva, J.E. Zucker, L.R. Carrion, C.H. Joyner, A.G. Dentai, IEEE J. Sel. Top. Quant. 6 (2000) 26.
[4] Y. Akage, K. Kawano, S. Oku, R. Iga, H. Okamoto, Y. Miyamoto, H. Takeuchi, Electron. Lett. 37 (2001) 299.
[5] G.B. Stringfellow, Organometallic Vapor-Phase Epitaxy: Theory and Practice, Academic Press, SanDiego, 1989.
[6] L. Samuelson, P. Omling, H.G. Grimmeiss, J. Cryst. Growth 61 (1983) 425.
[7] D.C. Law, L. Li, M.J. Begarney, R.F. Hicks, J. Appl. Phys. 88 (2000) 508.
[8] M.L. Hitchman, K.F. Jensen, Chemical Vapor Deposition: Principles and Applications, Academic, London, 1993.
[9] I. Kim, K. Uppal, W.-J. Choi, P.D. Dapkus, J. Cryst. Growth 193 (1998) 293.
[10] B.W. Liang, C.W. Tu, J. Appl. Phys. 74 (1993) 255.
[11] S.D. Adamson, B.-K. Han, R.F. Hicks, Appl. Phys. Lett. 69 (1996) 3236.
[12] B.-K. Han, L. Li, Q. Fu, R.F. Hicks, Appl. Phys. Lett. 72 (1998) 3347.
[13] D.C. Law, Y. Sun, R.F. Hicks, J. Appl. Phys., submitted for publication.
[14] M.J. Begarney, C.H. Li, D.C. Law, S.B. Visbeck, Y. Sun, R.F. Hicks, Appl. Phys. Lett. 78 (2001) 55.
[15] Y. Sun, S.B. Visbeck, D.C. Law, R.F. Hicks, Surf. Sci. 513 (2001) 256.
[16] R.L. Summers, Lewis Research Center, Cleveland, Ohio, NASA TN D-5285.
[17] L. Toben, T. Hannappel, K. Moller, H.-J. Crawack, C. Pettenkofer, F. Willig, Surf. Sci. 494 (2001) 755.
[18] W.G. Schmidt, F. Bechstedt, N. Esser, M. Pristovsek, Ch. Schultz, W. Richter, Phys. Rev. B 57 (1998) 14596.
[19] L. Li, Q. Fu, C.H. Li, B.-K. Han, R.F. Hicks, Phys. Rev. B 61 (2000) 10223.
[20] L. Li, B.-K. Han, Q. Fu, R.F. Hicks, Phys. Rev. Lett. 82 (1998) 1879.

[21] C. Theodoropoulos, N.K. Ingle, T.J. Mountziaris, Z.-Y. Chen, P.L. Liu, G. Kioseoglou, A. Petrou, J. Electrochem. Soc. 142 (1995) 2086.
[22] N.K. Ingle, C. Theodoropoulos, T.J. Mountziaris, R.M. Wexler, F.T.J. Smith, J. Cryst. Growth 167 (1996) 543.
[23] P. Cova, R.A. Masut, J.F. Currie, J. Phys. III 2 (1992) 2333.
[24] Q. Fu, L. Li, M.J. Begarney, B.-K. Han, D.C. Law, R.F. Hicks, J. Phys. IV France 9 (1999) 8.
[25] Q. Fu, L. Li, C.H. Li, M.J. Begarney, D.C. Law, R.F. Hicks, J. Phys. Chem. B 104 (2000) 5595.
[26] Q. Fu, E. Negro, G. Chen, C.H. Li, D.C. Law, R.F. Hicks, Phys. Rev. B 65 (2002) 75318.
[27] D.R. Lide (Ed.), CRC Handbook of Chemistry and Physics, 79th ed., CRC, Boca Raton, 1998.
[28] D.R. Stull, H. Prophet (Eds.), JANAF Thermochemical Tables, 2nd ed, US Government Printing Office, Washington, 1971.
[29] J.A. Dean (Ed.), Lange's Handbook of Chemistry, 15th ed., McGraw-Hill, New York, 1999.
[30] G. Chen, S.B. Visbeck, D.C. Law, R.F. Hicks, J. Appl. Phys. 91 (2002) 9362.
[31] W. Stolz, J. Cryst. Growth 209 (2000) 272.
[32] D. Keiper, R. Westphalen, G. Landgren, J. Cryst. Growth 204 (1999) 256.
[33] P. Velling, Prog. Cryst. Growth 41 (1–4) (2000) 85.